Applied Catalysis B: Environmental 323 (2023) 122043

Contents lists available at ScienceDirect

Applied Catalysis B: Environmental

journal homepage: www.elsevier.com/locate/apcatb

Sustained release catalysis: Dynamic copper releasing from stoichiometric spinel $CuAl_2O_4$ during methanol steam reforming

Ya-Jie Liu [a,1], He-Fei Kang [b,d,1], Xiao-Ning Hou [b], Shao-Jun Qing [b,*], Lei Zhang [c], Zhi-Xian Gao [c,*], Hong-Wei Xiang [b]

[a] Department of Chemistry and Chemical Engineering, Jinzhong University, Jinzhong 030619, China
[b] Institute of Coal Chemistry, Chinese Academy of Sciences, Taiyuan 030001, China
[c] College of Chemistry, Chemical Engineering and Environment Engineering, Liaoning Petrochemical University, Fushun 113001, China
[d] University of Chinese Academy of Sciences, Beijing 100049, China

ARTICLE INFO

Keywords:
Dynamic copper releasing
Stoichiometric spinel $CuAl_2O_4$
Methanol steam reforming
Sustained release catalysis

ABSTRACT

Dynamic copper releasing from a stoichiometric $CuAl_2O_4$ catalyst in methanol steam reforming (MSR) is investigated via detailed characterizations of six samples that are collected after testing for different time (*TOS*). It reveals that Cu can be liberated from spinel structure under the MSR conditions, serving as the active species. The Cu releasing rate increases first and then decreases with *TOS*, and the released Cu atoms agglomerate into nano entities. Consequently, the number of these Cu nanoparticles increases quasi-linearly with *TOS*, suggesting at least part of newly released Cu do not coalesce with the former nanoparticles but form new entities anchored on the surfaces of remnant defective Cu-Al spinel, which retains a small portion of Cu^{2+} (5.8%) in spinel lattice even at a prolonged *TOS* of 300 h. The findings evidence the dynamic changes of both active Cu metal and local surface structures, which are essentially different from conventional catalysis.

1. Introduction

Copper-based catalysts, which have been extensively applied in a variety of significant chemical applications, can be classified into two major categories according to the chemical bonding state of Cu: supported Cu-based catalysts (CuO/X, where X represents the catalyst supports, such as metal oxides, carbon materials, silica, zeolite, polymer, etc.) [1], and copper catalysts with special crystal structure, such as spinel-type [2–9], delafossite-type [10–12], perovskite-type [13–15], and layered double hydroxides [16–20].

For most of the copper catalysts, the low valence copper species (Cu^0 or Cu^+) have been claimed to be the active species [21–28]. Therefore, the as-synthesized copper catalysts are usually reduced before catalytic reaction to generate the required active copper centers, which is referred to as the conventional catalytic method. As such, the sizes of generated Cu nanoparticles (Cu NPs) were measured to be a few nanometers to tens of nanometers depending on the properties of catalyst precursors and the reduction conditions [29–36]. This occurrence suggests that copper sintering happens during the pre-reduction treatment process, which impairs copper utilization efficiency.

To cope with this problem, we have proposed the direct use of Cu-based spinel catalysts in methanol steam reforming (MSR) without pre-reduction treatment [37–39]. The active copper species are slowly released in situ during the catalytic reaction, and thus form more new active centers with time on stream (*TOS*). As a matter of fact, the catalytic performance of the copper spinel catalysts in MSR can be greatly enhanced as compared with the conventional pre-reduction method, and exhibits an obvious activity superiority to the commercial Cu-Zn-Al catalyst [37]. This new strategy of catalyst utilization has been named sustained release catalysis (SRC) in our previous papers [38,40].

Based on the concept of SRC, we have conducted a series of studies on copper-aluminate spinel catalytic materials. The Cu-Al spinel synthesis parameters, including the synthesis temperature and time, Cu/Al molar ratio, calcination atmosphere, different copper sources, and modification by the third components (Ni, Mg) were investigated in detail [38–44]. It has been found that the synthesis conditions strongly affected the physicochemical properties of Cu-spinel catalysts, such as crystal composition, catalyst reducibility, surface structure, cation

* Corresponding authors.
E-mail addresses: qingshaojun@sxicc.ac.cn (S.-J. Qing), gaozx@lnpu.edu.cn (Z.-X. Gao).
[1] These authors contributed equally to this work. All authors have given approval to the final version of the manuscript.

https://doi.org/10.1016/j.apcatb.2022.122043
Received 23 July 2022; Received in revised form 14 September 2022; Accepted 3 October 2022
Available online 4 October 2022
0926-3373/© 2022 Published by Elsevier B.V.

distribution, and so on, and these properties co-determined the catalytic performance in MSR.

Oxide spinel has a face-centered cubic crystal structure arranged by anion O^{2-} ions, which contains both tetrahedral and octahedral interstices. Both divalent and trivalent metallic cations can be distributed in these interstices [45]. Used as the sustained release catalysts, Cu-based spinel materials have huge advantages due to their special crystal structure. The catalytic behavior of Cu-Al spinel is featured by an activity increase in the early period of the reaction and a gradual activity decrease when most spinel copper species have been released.

Therefore, it can be deduced that the copper releasing rate dramatically influences catalytic performance in the SRC systems. When a portion of Cu atoms are being released from the spinel structure, both Cu^{2+} and Al^{3+} cations in the spinel structure will redistribute simultaneously, leading to the revolution of surface defective spinel structure. This hypothesis implies that the catalyst microstructure may change constantly during the reaction process, which makes the sustained release catalytic system extremely complex.

Up to now, the dynamics of copper releasing from the spinel structure remain unclear. Based on our preliminary investigations, a stoichiometric $CuAl_2O_4$ spinel and a spinel solid solution with excessive Al^{3+} ions should be selected to study the copper releasing dynamics in MSR. Both spinel samples have different physicochemical properties and thus show different catalytic behaviors. In this report, the dynamics of copper releasing from a stoichiometric $CuAl_2O_4$ spinel are focused on. The releasing features of spinel Cu, structure revolution of the defect spinel, clarification for the catalytic behavior, and dynamics of the sustained release process are discussed. The findings of this work have revealed a dynamic catalytic process system that is essentially different from the conventional catalysis with pre-reduction treatment, providing basic data for further investigations of the SRC.

2. Experimental

2.1. Catalyst preparation

The fresh stochiometric $CuAl_2O_4$ spinel sample was prepared by a simple solid-phase method at 1200 °C with an atomic ratio of Al/Cu = 3. It has been illustrated to be a composite of $CuAl_2O_4$ spinel and 1/2 α-Al_2O_3 phase [39,44]. By using the fresh sample in MSR for different *TOS*, six intermediate tested samples with 4 h, 5 h, 7 h, 29 h, 100 h and 300 h were obtained. Herein, the tested samples are signed by *TOS* and the fresh stoichiometric $CuAl_2O_4$ spinel is marked as 'fresh'.

2.2. Catalyst characterization

Temperature programmed reduction with hydrogen (H_2-TPR) was carried out on a Finetec Finesorb-3010 chemisorption analyzer. For a normal H_2-TPR experiment, 30.0 mg sample was loaded in a fixed-bed U-type quartz tube reactor. 10% H_2/Ar with a volumetric flow rate of 15 ml min^{-1} was selected and the temperature was heated from room temperature (*RT*) to 900 °C at a heating rate of 10 °C min^{-1}. For all tested samples, a pre-oxidization treatment was carried out in 5% O_2/Ar at 280 °C to transform low valence copper species into divalent Cu^{2+}. XPS measurements were performed on an X-ray photoelectron spectrometer (AXIS ULTRA DLD) with Al Kα radiation (1486.8 eV) at an energy resolution of 0.48 eV (Ag 3d5/2). The binding energies of Cu 2p, Cu LMM and Al 2p were calibrated by the C 1 s peak (BE = 284.8 eV).

Powder X-ray diffraction (XRD) patterns of the spinel samples were measured on a Rigaku X-ray diffractometer with Cu-Kα radiation. The scanning ranged from 10° to 80° of 2theta with a step size of 0.02° at 4 °C min^{-1}. Cu L_3-edge x-ray absorption near edge structure (Cu L_3-edge XANES) was characterized with a Monk-Gillieson monochromator at beamline 4B7B endstation of Beijing Synchrotron Radiation Facility (BSRF). A 2.5 GeV ring energy and a 250 mA maximum stored current were used to provide an energy range of 50–1700 eV for soft x-ray experiments. For each measurement, the vacuum was kept at about 8.5 × 10^{-6} Torr. All tested samples were pre-oxidized to transform low valence copper species into divalent Cu^{2+}. The Cu $2p_{3/2}$ peak of CuO phase at 931.3 eV was used in calibrating all absolute energy data [46]. In peak deconvolution analysis, peak positions were intentionally fixed to obtain good fitting results. The spectra reflect the chemical state of copper in the catalyst out-layer (surface and near-surface) [47]. ^{27}Al magic angle spinning nuclear magnetic resonance spectroscopy (^{27}Al MAS NMR) was measured by a Bruker Avance 600 spectrometer in a nominal field of 14.2 T. The equipped magic angle spinning probe contained a 4.0 mm ZrO_2 rotor and operated at a rotation frequency of 13 kHz. The excitation length and interval of pulse were determined to be 0.4 μs and 1 s, respectively. All chemical shift values were calibrated by the data of $Al(NO_3)_3$ solution at 0 ppm.

N_2O titration of active copper was carried out on a Finetec Finesorb-3010 chemisorption analyzer. For a typical measurement, two steps were performed as shown below. Firstly, the tested samples were oxidized by 5% N_2O/Ar (15 ml/min) at 50 °C for 20 min, then reduced by 10% H_2/Ar (15 ml min^{-1}) from *RT* to 220 °C at 10 °C min^{-1}, and the reduction peak area was denoted as H_{Cu_2O}; Secondly, the tested samples were oxidized in air at 280 °C for 30 min, then reduced in 10% H_2/Ar (15 ml min^{-1}) from *RT* to 280 °C at 10 °C min^{-1}, and the reduction peak area was denoted as H_T. Then, the copper dispersion (D_{Cu}), copper surface area (S_{Cu}) and average Cu diameter ($d_{Cu}^{N_2O}$) can be calculated by the following equation: [36].

$$D_{Cu} = 2 \times H_{Cu_2O}/H_T \times 100\%$$

$$S_{Cu} = 2 \times H_{Cu_2O} \times N_{av}/(H_T \times M_{Cu} \times 1.4 \times 1019) = 1353 \times H_{Cu_2O}/H_T \quad (m^2Cu/g\ Cu)$$

$$d_{Cu}^{N_2O} = 6/(S \times \rho_{Cu}) \approx 0.5 \times H_T/H_{Cu_2O} \quad (nm)$$

where H_{Cu_2O} and H_T are H_2 consumptions of Cu_2O and total copper oxide, respectively; M_{Cu} = 63.46 g mol^{-1}, N_{av} = Avogadro's constant, ρ_{Cu} = 8.92 g cm^{-3}. Besides, several times for a N_2O titration experiment were performed to control the weighing error.

High-resolution transmission electron microscopy (HRTEM) was performed on a Tecnai G2 F20 S-Twin using field emission scanning. The average particle size of Cu NPs is calculated using the volume-surface diameter equation as:

$$d_{Cu}^{TEM} = \sum n_i d_i^3 \Big/ \sum n_i d_i^2$$

where n_i is the number of particles with a characteristic diameter d_i.

A TG-MS method was used to characterize the carbon deposit. A typical run was performed from *RT* to 550 °C at 3 °C min^{-1} in 5% O_2/Ar. For the comparison, the tested $CuAl_2O_4$ spinel with 300 h was also tested in pure He with the same temperature procedure. N_2-physisorption analysis was carried out on a nitrogen adsorption system (Tristar 3000) at about − 196 °C. Each sample was degassed at 80 °C for 1 h before analysis. The surface areas were measured by the Brunauer-Emmett-Teller (BET) method in the partial pressure range of 0.05–0.30. The pore volumes and average pore diameters were measured by the Barrett-Joiner-Halenda (BJH) method based on the adsorption isotherms.

2.3. Catalytic testing

A conventional fixed bed reactor was used to evaluate the catalytic performance of the $CuAl_2O_4$ spinel catalyst in MSR. The as-synthesized catalyst powder was pressed, crushed, and sieved to a particle size range of 1.4–2.5 mm. The reaction conditions of MSR are as follows: temperature 210–300 ℃, pressure 1.0 Mpa, weight hourly space velocity *WHSV* = 2.18 h^{-1}, methanol to water is 0.442 (molar ratio).

The reaction effluents were cooled in a condenser to separate the liquid and gas products. Two gas chromatographers equipped with a

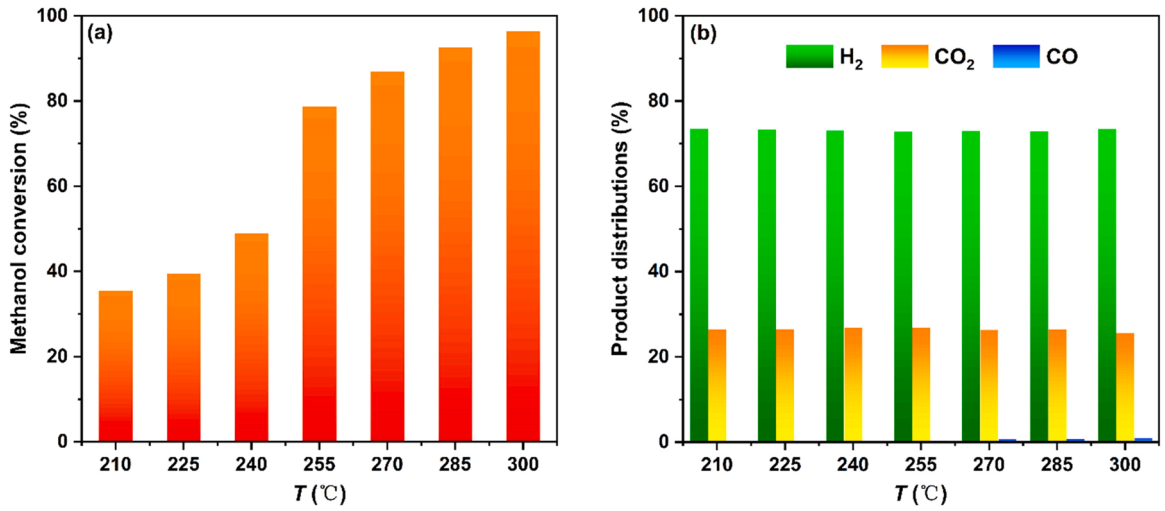

Fig. 1. Methanol conversion (a) and product distributions (b) in MSR at the different reaction temperatures.

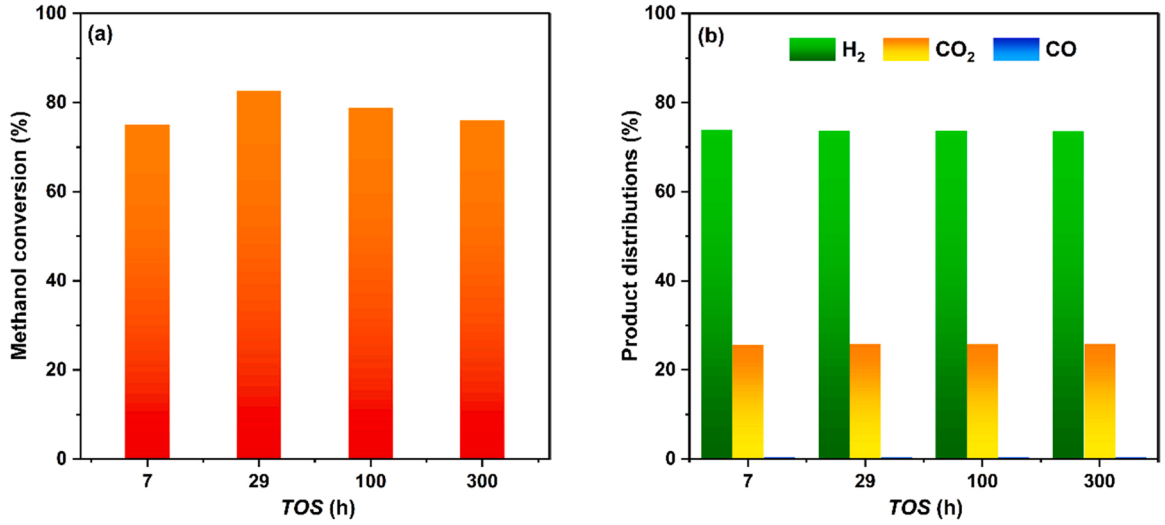

Fig. 2. Methanol conversion (a) and product distributions (b) in MSR at different *TOS*.

porapak T column and a carbon molecular sieve column, respectively, were used to analyze the products. The analysis results of both liquid and gas products were integrated to calculate product distributions.

The product distributions and CH_3OH conversion are denoted as follows:

$$\text{Product distributions}(\%) = \frac{F_i(i = H_2, CO, CO_2)}{F_{CO} + F_{CO_2} + F_{H_2}} \times 100\% \quad (1)$$

$$CH_3OH \text{ conversion}(\%) = \frac{F^{in}_{CH_3OH} - F^{out}_{CH_3OH}}{F^{in}_{CH_3OH}} \times 100\% \quad (2)$$

where, $F^{in}_{CH_3OH}$ and $F^{out}_{CH_3OH}$ represent the influent and effluent molar flow rate of CH_3OH, F_{H_2}, F_{CO} and F_{CO_2} are the effluent molar flow rate of H_2, CO and CO_2, respectively.

3. Results

3.1. Catalytic performance

The as-synthesized stoichiometric $CuAl_2O_4$ spinel catalyst is tested in MSR without pre-reduction. To explore the reaction temperature dependence of catalytic performance in MSR, the $CuAl_2O_4$ spinel is tested in the temperature range of 210–300 °C. As shown in Fig. 1a, the methanol conversion is about 35% at 210 °C and it exceeds 95% at 300 °C, showing a gradual increase with the enhanced reaction temperature due to the endothermic equilibrium-limited nature of the MSR reaction. In this catalytic system, the products are mainly composed of 73.0–74.0% H_2 and 25.5–26.5% CO_2. A trace amount of CO (<1.0%) is detected simultaneously, showing a slight increase with the reaction temperature rise (Fig. 1b).

To investigate the sustained release catalytic behavior of the $CuAl_2O_4$ spinel with reaction time, an optimal reaction temperature of 255 °C is selected for long-term catalytic testing. As can be seen in Fig. 2a, methanol conversion increases from 7 h to 29 h, then decreases slowly in the *TOS* range of 29–300 h, exhibiting a typical catalytic behavior of Cu-Al spinel catalysts via the SRC method in MSR [39]. Besides, the fractions of H_2, CO_2 and CO are determined to be about 73.6%, 25.9% and 0.5%, respectively (Fig. 2b).

3.2. Releasing process

3.2.1. H_2-TPR studies

Fig. 3 shows the H_2-TPR profiles of both the fresh stoichiometric

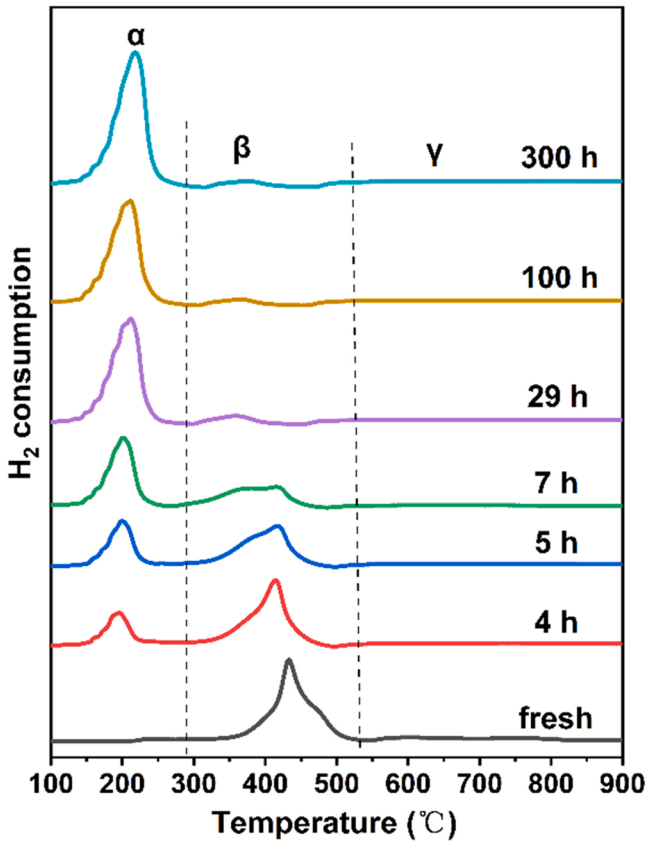

Fig. 3. H_2-TPR profiles of the fresh spinel sample and pre-oxidized tested spinel samples.

$CuAl_2O_4$ spinel sample and six intermediate samples tested in MSR for different *TOS*. For all the tested samples, a pre-oxidation treatment up to a maximum temperature of 280 °C is carried out, aiming to oxidize the copper metal phase into divalent CuO species. According to our previous papers [39,41], the H_2-TPR profiles of Cu-Al spinel catalysts can be divided into three zones, namely α (150–280 °C), β (280–530 °C) and γ (530–900 °C). The α with a lower temperature is the reduction of non-spinel Cu^{2+} species that may include free CuO and/or Cu-O-Al intermediate [41]. For the fresh $CuAl_2O_4$ sample prepared at a high temperature of 1200 °C, the α reduction is pretty small and mainly belongs to the reduction of Cu-O-Al intermediate species [41]. However, for other tested samples that have been pre-oxidized, it can be ascribed to the reduction of free CuO phase and maybe a small portion of Cu-O-Al intermediate. β and γ are both attributed to the reduction of spinel Cu^{2+}, denoting easy-reducible spinel Cu^{2+} and hardly-reducible spinel Cu^{2+}, respectively [39]. The γ peak is relatively flat and the enlarged graph is provided in Fig. S1. Obviously, the reduction of spinel Cu^{2+} occurs in a wide temperature range of 280–900 °C.

Compared with the fresh sample, the β peaks of tested samples shift to lower temperatures, and the full width at half maxima becomes wider (Table S1, Fig. S1). It should be noted that the intensity of peak β decreases while that of peak α increases with *TOS*, indicating the continuous release of spinel Cu during MSR. To calculate the releasing degree of spinel copper (*RD*), area integration analysis is performed with the H_2-TPR profiles. As can be observed in Table 1, a longer reaction time leads to a higher *RD*. Within the initial 29 h, more than 91% spinel Cu^{2+} ions are released, and the release rate drops dramatically afterward. Importantly, a small portion of copper species (about 5.8%) still exists in the spinel structure even after long-term testing of 300 h. Hence, the average release rate (Table 1) is calculated to gain more understanding of the releasing features, and the detailed explanations are given in the discussion Section 4.1. When copper is released from the spinel structure, the stoichiometric $CuAl_2O_4$ spinel will transform into a copper-deficient spinel solid solution, i.e., defective spinel. Accordingly, a series of Cu-deficient spinel solid solutions with different Cu/Al atomic ratios are formed during the releasing process, suggesting the dynamic change of the catalyst.

3.2.2. XPS studies

XPS studies are conducted to investigate the variation of surface Cu species in both the fresh and tested samples. For the fresh $CuAl_2O_4$ spinel sample, Cu 2p signals (at 933.1 eV and 935.0 eV) and the strong satellite peaks (Fig. 4a) reveal the characters of divalent Cu^{2+} in non-spinel and spinel phase, respectively [48–52]. Peak fit analysis (Table 1) reveals that surface Cu^{2+} in the fresh $CuAl_2O_4$ spinel sample is composed of 99.5% spinel Cu^{2+} and 0.5% non-spinel CuO.

For the tested samples, the released Cu species should exist as Cu metal. As shown in Fig. 4a, the Cu 2p main peaks shift toward lower binding energy positions, and the satellite peaks of Cu 2p signals decrease sharply. The Cu $2p_{3/2}$ main peak can be deconvoluted into two peaks at about 932.6 eV and 935.0 eV (Fig. 4a), ascribing to non-spinel Cu species (including low valence Cu^0, Cu^+ and Cu^{2+}) and spinel Cu^{2+}, respectively [48–52]. Further evidence from Cu LMM signals at 916.2 eV and 918.3 eV shows that both Cu^+ and Cu^0 exist in tested samples (Fig. 4b). Because divalent Cu^{2+} in the fresh sample will be gradually reduced to Cu metal during the MSR reaction, the appearance of Cu^+ species in tested samples may be attributed to the oxidation of Cu^0 when the sample is exposed to air during the sample transfer process.

Compared with the fresh sample, the content of surface spinel Cu^{2+} in tested samples decreases gradually, indicating the dynamic release of copper from spinel structure. Specifically, a sharp decrease of surface spinel Cu^{2+} from 98.5% to 19.7% is found in the initial 4 h, and afterwards the releasing of surface spinel Cu^{2+} becomes very slow, especially from 100 h to 300 h (Table 1). Consequently, the surface Cu/Al ratio (Table 1), calculated from Cu 2p and Al 2p peak area (Fig. 4a, c), shows a

Table 1
Properties of the fresh and tested spinel solid solution samples.

Sample	Fresh	4	5	7	29	100	300
Bulk phase (H_2-TPR)							
X[Spinel Cu^{2+}] (%)[a]	99.8	73.8	60.6	44.6	8.9	7.1	5.8
RD (%)[b]	0	26.2	39.4	55.4	91.1	92.9	94.2
r[Spinel Cu^{2+}] (% h^{-1})[c]	/	6.55	13.20	8.00	1.62	0.025	0.0065
Surface phase (XPS)							
Y[Spinel Cu^{2+}] (%)[d]	98.5	19.7	18.1	15.6	14.8	10.1	9.9
(Cu/Al)[e]	0.181	0.210	0.232	0.245	0.279	0.276	0.273

[a] Molar ratio of spinel Cu^{2+} to all Cu in the bulk phase.
[b] Cu releasing degree.
[c] Cu average releasing rate during t_{i-1}-t_i.
[d] Molar ratio of spinel Cu^{2+} to all Cu in the surface phase.
[e] Surface Cu/Al molar ratio.

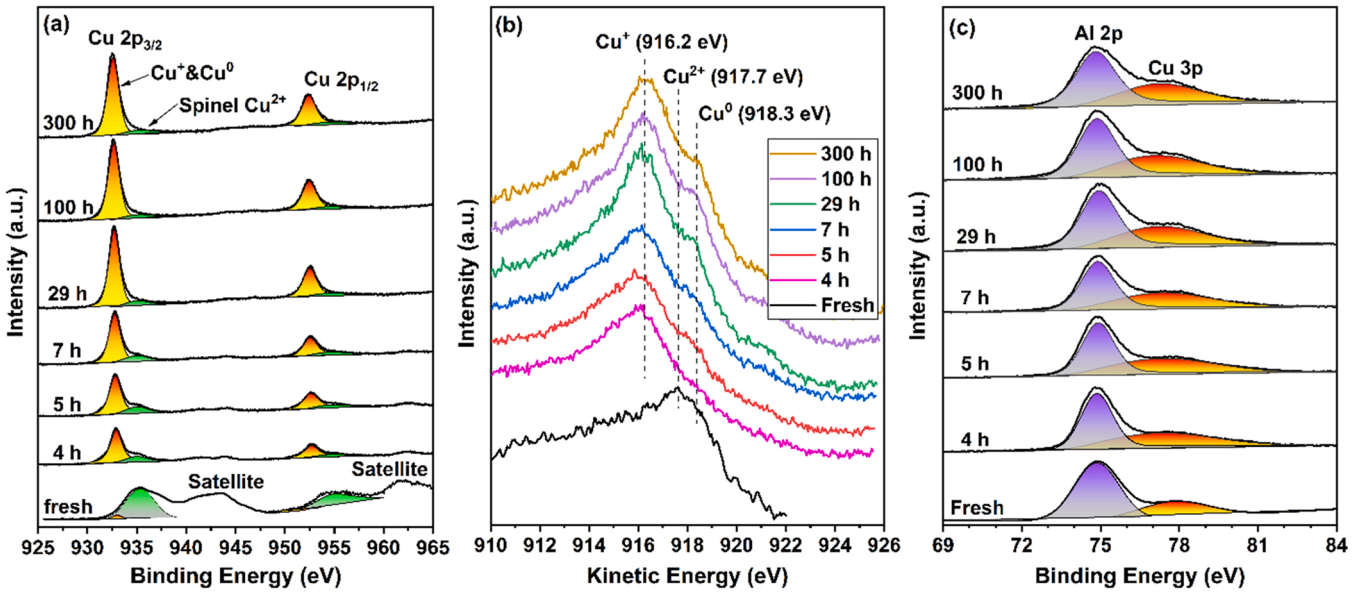

Fig. 4. XPS spectrums of Cu 2p (a), Cu LMM (b), Al 2p&Cu 3p (c) of fresh sample and tested samples.

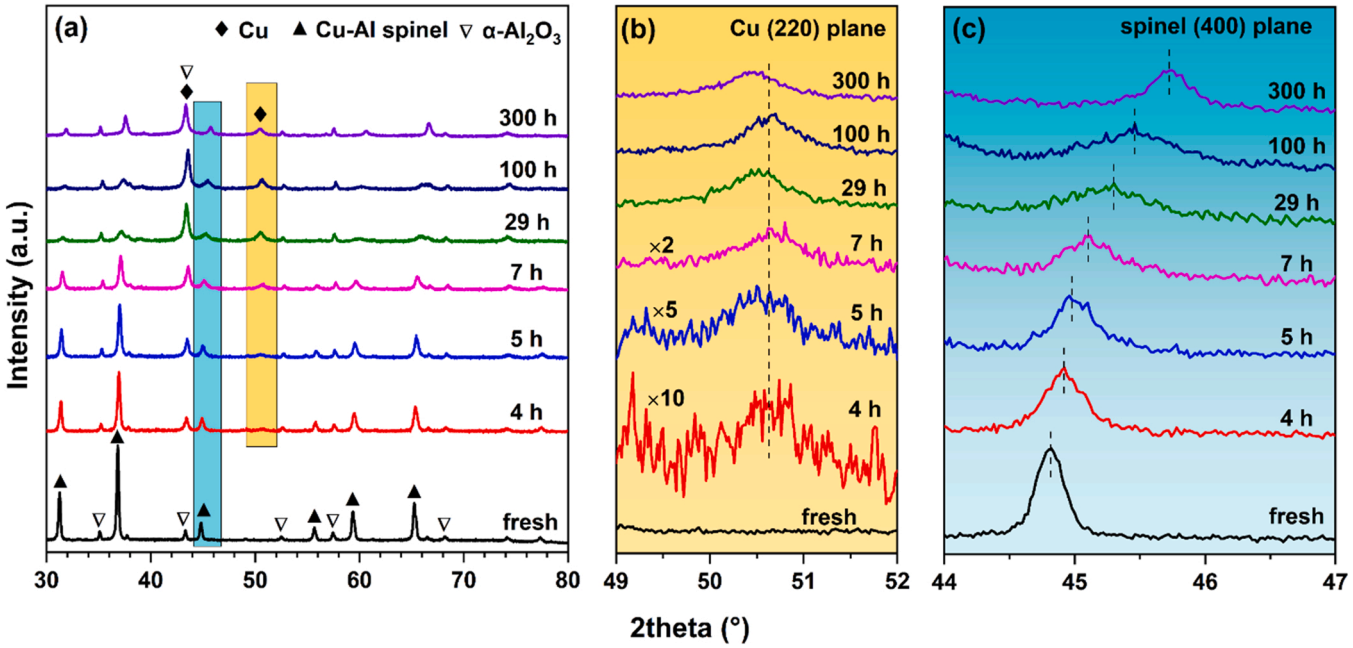

Fig. 5. XRD patterns of the fresh sample and tested samples (a), enlarged Cu (220) lines (b), and enlarged spinel (400) lines (c).

constant increase before 25 h and a slight decrease in 25–300 h, which can be attributed to the combined effect of Cu releasing and agglomeration. It is noted that about 9.9% spinel Cu^{2+} remain in the catalyst surface layer at 300 h (Table 1), indicating the high stability of Cu-Al surface spinel, as also illustrated by the Cu-Ni-Al [38] and Cu-Mg-Al [43] surface spinel in our previous papers. It should be mentioned that the Cu-Al surface spinel plays a key role in stabilizing the active Cu NPs as compared to γ-Al_2O_3[39], which is also supported by the theoretical calculations [53].

3.3. Structural properties

3.3.1. XRD studies

XRD patterns of fresh and tested samples with different *TOS* are shown in Fig. 5. By comparing with the ICSD files, the crystalline phase of stoichiometric $CuAl_2O_4$ is identified in the fresh sample, whose cell constant of 8.076 Å is very close to that of ICSD #24491 ($CuAl_2O_4$, a = 8.075 Å). Six main diffraction lines of Cu-Al spinel phase distribute in the 2theta range of 30°– 70°. Besides, α-Al_2O_3 phase (ICSD #85137) is detected in the fresh sample, which is attributed to the precipitation of excessive Al^{3+} ions as the synthetic precursor has an atomic ratio of CuAl = 1/3. Our previous investigation has demonstrated that excessive Al would precipitate out as α-Al_2O_3 phase from Al-rich Cu-Al spinel solid solution upon increasing the calcination temperature and/or synthetic duration [39,41,44]. It is noteworthy that α-Al_2O_3 phase is very stable [54,55] and remains unchanged during the MSR process as indicated by its constant XRD diffraction lines at different *TOS* (Fig. 5a).

With all tested samples, the diffraction lines at 2θ of 43.3° and 50.5° (Fig. 5a) can be ascribed to (111) and (220) crystal planes of Cu metal (ICSD #53247), respectively. However, the diffraction line of Cu metal

Table 2
Properties of the fresh and tested spinel solid solution samples.

TOS	Fresh	4	5	7	29	100	300
a_{spinel} (Å)[a]	8.076	8.066	8.048	8.027	8.007	7.965	7.943
d_{spinel} (nm)[b]	33.8	27.4	24.1	18.1	11.9	13.3	19.6
x in $[Cu_{1-3x}V_xAl_{2+2x}O_4]$[c]	0	0.145	0.175	0.213	0.307	0.313	0.316
$I_{(220)}/I_{(400)}$[d]	2.80	2.37	2.45	1.92	0.57	0.39	0.79
d_{Cu}^{XRD} (nm)[e]	/	11.0	10.9	10.6	10.4	10.4	10.3
$d_{Cu}^{N_2O}$ (nm)[f]	/	9.3	9.2	8.9	8.5	8.5	8.6

[a] Cu-Al spinel cell parameters.
[b] Average crystalline sizes of Cu-Al spinel.
[c] 'x' was determined by H_2-TPR results.
[d] Intensity ratio of (220) line to (440) line of Cu-Al spinel.
[e] Average crystalline sizes of Cu nanoparticles obtained by XRD method.
[f] Average crystalline sizes of Cu nanoparticles obtained by N_2O titration method.

(111) plane is coincidently overlapped with that of α-Al_2O_3 (113) plane (Fig. 5a), thus Cu metal analysis will be performed in terms of (220) plane solely (Fig. 5b). It is shown that the diffraction intensity of Cu (220) line increases with *TOS*, demonstrating the dynamic releasing of Cu atoms from spinel structure in MSR. The released Cu atoms will coalesce into Cu NPs during the reaction process due to the easy-sintering nature of copper. The average crystal size of Cu NPs (d_{Cu}^{XRD}, Table 2), calculated by the Scherrer equation, decreases slightly from 11.0 nm to 10.3 nm during the 300 h catalytic testing of MSR, and such variation trend is further confirmed by N_2O titration and HRTEM method (Section 3.4), and will be correlated to the release behavior in the discussion section.

To investigate the variation of the spinel phase during the MSR reaction process, the spinel (400) plane is selected and the diffraction lines are enlarged as shown in Fig. 5c. The diffraction peaks shift toward higher 2theta values with increasing *TOS*, evidencing the formation of Cu-deficiency spinel solid solutions $Cu_{1-3x}V_xAl_{2+2x}O_4$ (*V*: Vacancy) with unequal Cu/Al atomic ratios at different *TOS* (Table 2). By using the six main diffraction lines, the cell constant of the spinel phase is calculated to decrease continuously from 0 h to 300 h, and a rapid decline from 29 h to 300 h can be noted (Table 2, Fig. S2). The spinel crystal size (Table 2) shows a decrease before 29 h (from 33.8 nm to 11.9 nm) and an increase between 29 and 300 h (from 11.9 nm to 19.6 nm), which may owe to the combined effect of Cu releasing and rearrangement of Al^{3+} ions. To sum up, the decrease of spinel cell constant has confirmed the gradual releasing of copper atoms and the formation of Cu-deficiency spinel solid solutions during MSR.

Apart from the peaks shift, the line intensity of the spinel phase decreases with increasing *TOS*. Importantly, the relative intensity of the characteristic diffraction lines also changes accordingly. For instance, the I_{220}/I_{400} declines from 2.80 to 0.39 and then slightly increases to 0.79 at 300 h (Table 2). Because the spinel diffraction patterns have tight connections with cation distribution in octahedral or tetrahedral interstices of the spinel structure [56], the results reflect the occurrence of cation redistribution in spinel structure when the spinel Cu^{2+} ions are gradually freed, which is further proved by following Cu L_3-edge XANES and ^{27}Al MAS NMR characterizations.

3.3.2. *Cu L_3-edge XANES studies*

To characterize Cu^{2+} coordination of Cu-Al spinel phase during the Cu releasing process in MSR reaction, Cu L_3-edge XANES analysis is carried out at the soft x-ray beamline endstation of BSRF. Because the electric structure of Cu^{2+} has a higher unoccupied 3d orbit that can receive an excited electron from $2p_{3/2}$ orbit, Cu L_3-edge absorption

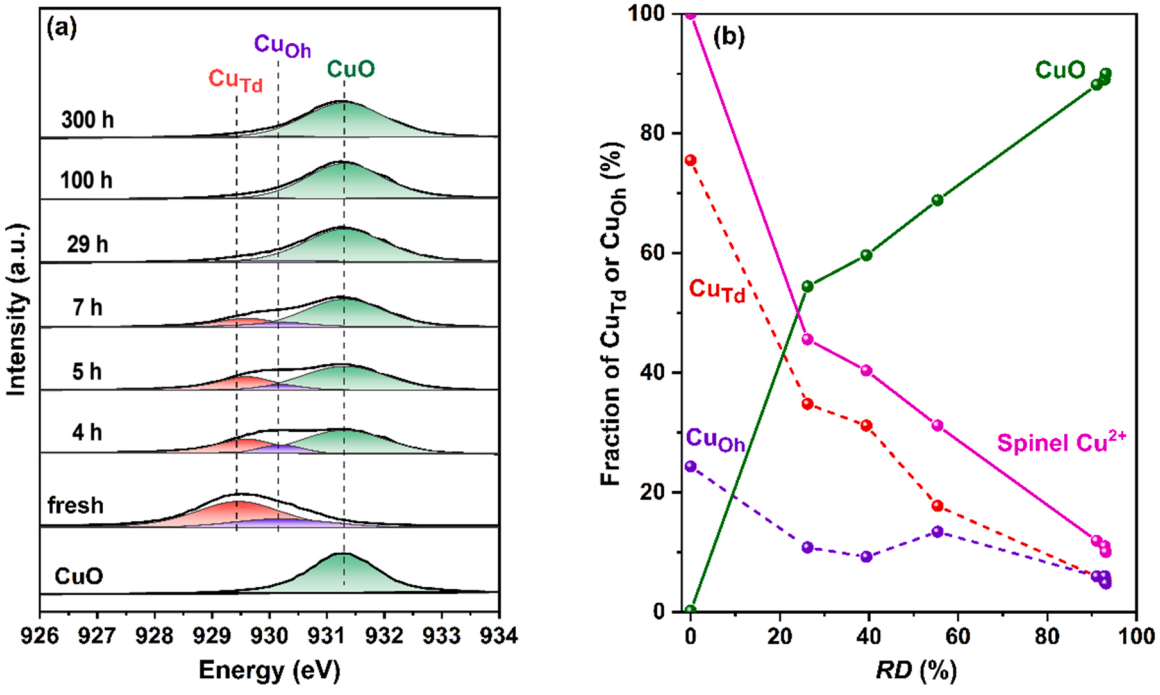

Fig. 6. Cu L_3-edge XANES spectra of CuO, the fresh and tested samples (a) and the fraction of Cu_{Td} or Cu_{Oh} as a function of *RD* (b).

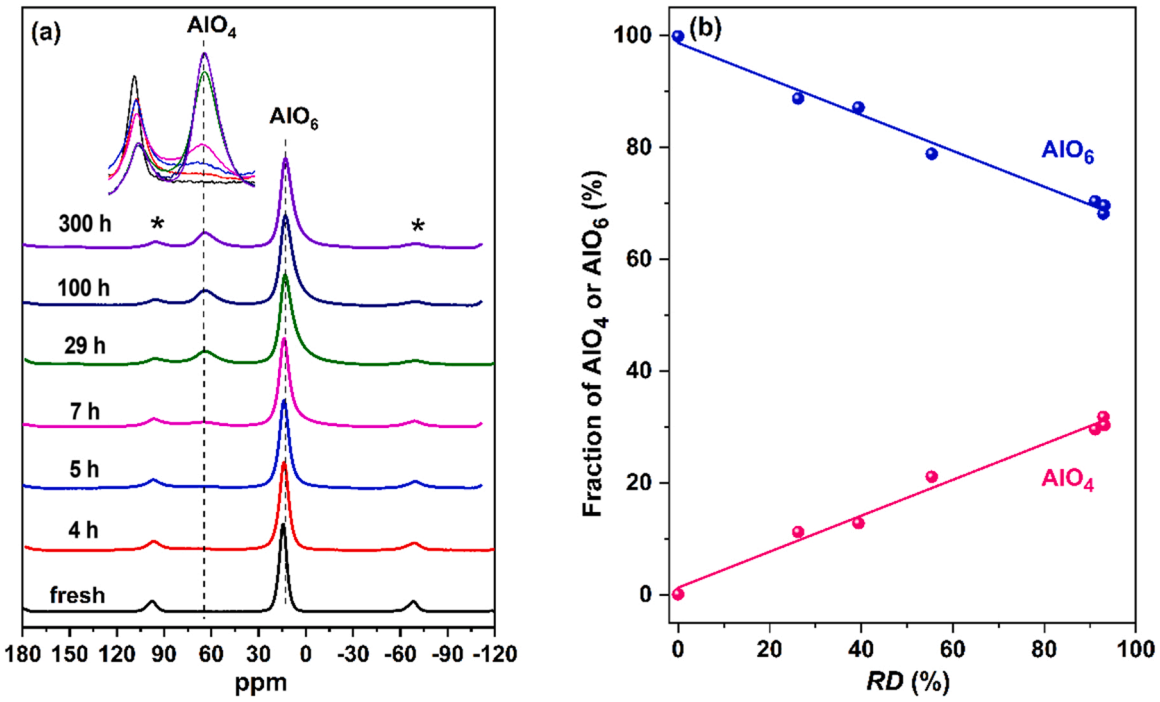

Fig. 7. ^{27}Al MAS NMR spectra of the fresh sample and tested samples (a) fraction of AlO_4 or AlO_6 as a function of *RD* (b).

peaks will provide typical features of $2p_{3/2}$→3d transition, which is capable to quantified the Cu^{2+} coordinations in catalyst out-layer [47, 57,58].

Fig. 6a shows Cu L_3-edge absorption peaks of fresh $CuAl_2O_4$ spinel and tested samples. The tested samples are pre-oxidized at 280 °C aiming to transform copper metal into divalent CuO. All the spectra show white line features owing to the transition from $2p_{3/2}$ level to unoccupied 3d state of Cu^{2+}. The obtained spectra can be deconvoluted to three peaks centered at 931.3 eV, 930.2 eV and 929.6 eV, corresponding to free CuO, octahedral spinel Cu^{2+} (Cu_{Oh}) and tetrahedral spinel Cu^{2+} (Cu_{Td}), respectively [38,57]. As shown in Fig. 6a, b and Table S2, the spinel Cu^{2+} content in the catalyst out-layer decreases whereas the free CuO content increases continuously with *TOS*. This result demonstrates the continuous releasing of copper atoms from spinel framework in MSR. It should be noted, however, with a long-term *TOS* of 300 h, about 10% spinel Cu^{2+} still exist in the catalyst out-layer, while only about 5.8% spinel Cu^{2+} ions remain in the bulk (Table 1). Hence, it can be said that a large proportion of remnant Cu^{2+} ions situate in the catalyst out-layer which forms the Cu-deficient surface spinel.

Interestingly, most of the spinel Cu^{2+} ions in the out-layer of fresh spinel sample are tetrahedrally coordinated, and these spinel Cu^{2+} ions exhibit a higher releasing rate during the releasing process (Fig. 6b). This result is consistent with previous literature research findings [59, 60]. For example, L.M. Plyasova et al. have found that tetrahedral spinel Cu^{2+} ions can be reduced below 270 °C by hydrogen while the reduction of octahedral spinel Cu^{2+} begins above 300 °C [59]. W.S. Xia et al. have illustrated that the surface bonding strength of Cu^{2+} ion lived in octahedral interstice is greater than that in tetrahedral interstice [60]. The above results have illustrated the relatively easier reducibility of tetrahedral spinel Cu^{2+} ions as compared to octahedral spinel Cu^{2+} in stoichiometric $CuAl_2O_4$ spinel. As a consequence, the distribution of Cu^{2+} cations in the catalyst out-layer would vary with *TOS*, which implies that out-layer Al^{3+} cations coordination may take place simultaneously. If so, how about the cation distribution in the bulk phase? To elucidate this issue, ^{27}Al MAS NMR has been performed as shown below.

3.3.3. ^{27}Al MAS NMR studies

Fig. 7 exhibits the ^{27}Al MAS NMR spectra of fresh $CuAl_2O_4$ spinel and tested samples. Two resonance signals centered at about 12.0 ppm and 65.0 ppm are observed in all spectra of the tested samples, which can be ascribed to octahedral Al^{3+} and tetrahedral Al^{3+} ions, respectively. The peaks signed by the asterisks are sideband peaks. As can be seen in Fig. 7a, the fresh spinel sample only contains octahedral Al^{3+} ions. Since the fresh sample contains 33.2% α-Al_2O_3 which only has six-coordinated octahedral Al^{3+} ions, it also contributes to the signal at 12.0 ppm [44].

With *TOS* increasing, the content of octahedral Al^{3+} decreases while the tetrahedral Al^{3+} content increases, indicating that the redistribution of Al^{3+} ions in spinel structure occurs when copper atoms are being released. By peak integration analysis, the fractions of both coordinated Al^{3+} are obtained (Table S3) and graphed versus *RD* (Fig. 7b). It is obvious that a quasilinear decrease or increase occurs in octahedral Al^{3+} and tetrahedral Al^{3+} ions, respectively.

Notably, the redistribution of Al^{3+} ions happens mainly in the first 29 h testing period, and after that only slight redistribution occurs. For example, the ratio of octahedral Al^{3+} decreases sharply from 100% to 70.4% in the first 29 h, while it changes slightly between 70.4% and 68.2% in the *TOS* range of 29 h to 300 h. According to H_2-TPR and Cu L_3-edge XANES results, the releasing of spinel Cu^{2+} slows down sharply after 29 h simultaneously. Therefore, it can be deduced that the cation redistribution has close relationships with the releasing of spinel Cu^{2+} ions, as also supported by the variation of intensity of XRD diffraction lines (Table 2).

3.4. Properties of Cu nanoparticles

3.4.1. N_2O titration

The above H_2-TPR, XPS and XRD characterizations have confirmed the copper releasing phenomenon from $CuAl_2O_4$ spinel during the MSR reaction. The released Cu atoms will agglomerate to Cu entities that may include Cu atoms, clusters and nanoparticles. As a matter of fact, separated Cu atoms or small Cu clusters cannot be identified by XRD [61], hence N_2O titration experiments are performed to measure copper dispersion (D_{Cu}), copper surface area (S_{Cu}) and average diameter of Cu entities ($d_{Cu}^{N_2O}$).

For all N_2O titration measurements, the reduction peak area of

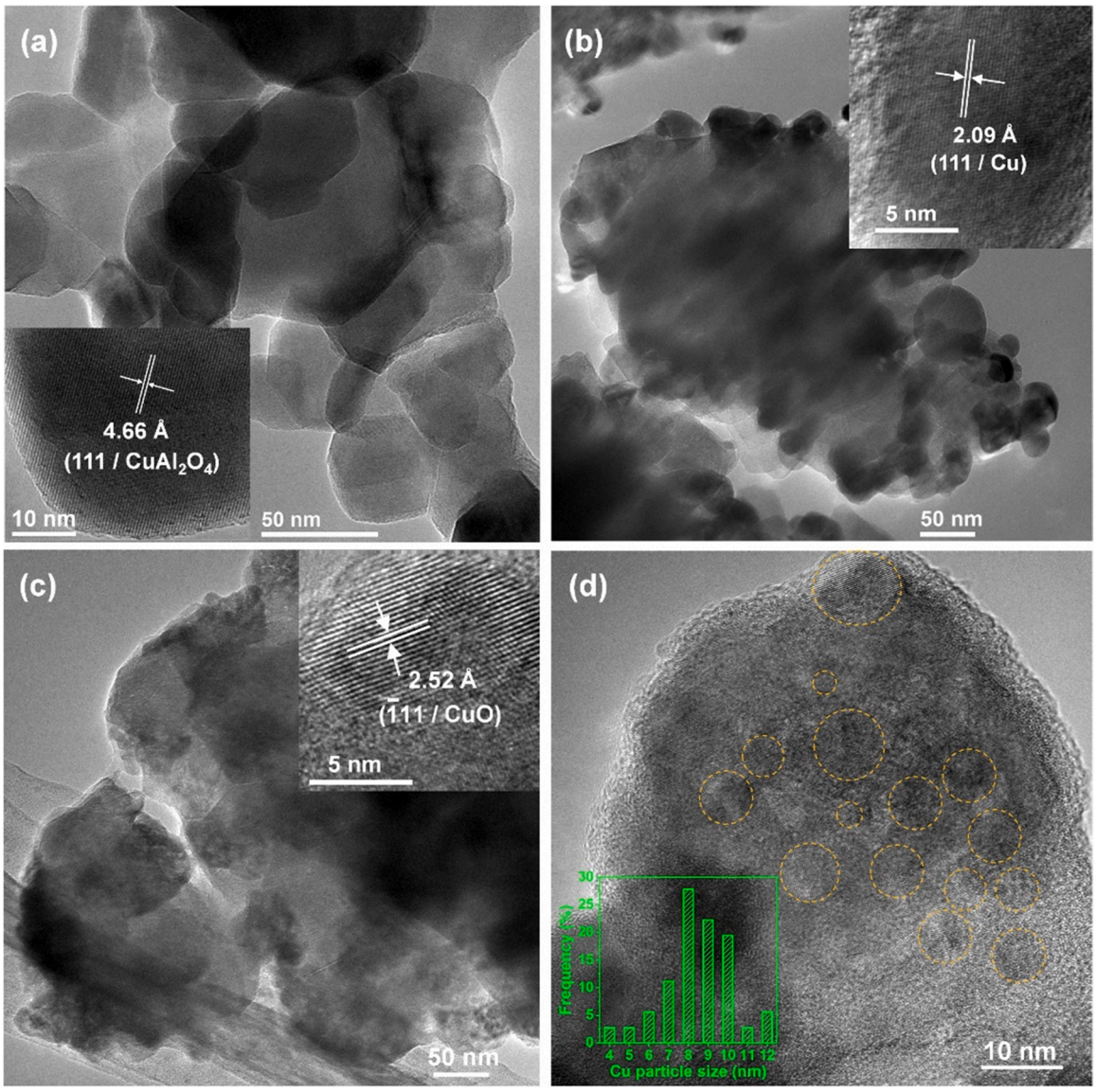

Fig. 8. HRTEM images of the fresh spinel sample (a), the tested samples with 100 h *TOS* (b) and the oxidized tested samples with 100 h *TOS* (c, d).

monovalent Cu^+, formed by oxidation with 5%N_2O/Ar, increases gradually with *TOS* as shown in Fig. S3, indicating the increased Cu released from spinel lattice during MSR process. With the copper *RD* increasing, the copper dispersions and surface areas are measured to be 10.8–11.8% and 72.9–79.7 m^2/g, respectively (Table S4). Importantly, the Cu diameters obtained from N_2O titration method show a decreasing trend with increasing *RD*, ranging between 8.5 and 9.3 nm (Table 2), and this phenomenon will be detained in the discussion section. From Table 2, one can find that the above calculated value is smaller than that from XRD results (10.3–11.0 nm). Hence, it is deduced that the Cu entities in tested spinel catalysts have a wide size distribution, which is also supported by the HRTEM results below. This finding can be expected to reflect the Cu releasing feature more precisely.

3.4.2. *HRTEM studies*

To further investigate the copper releasing from $CuAl_2O_4$ spinel, two selected samples, the fresh spinel sample and a sample tested for 100 h, are characterized by HRTEM technique. The fresh spinel sample shows clear contours with different shapes, and the lattice fringes with an interplanar spacing of 4.66 Å can be ascribed to (111) plane of $CuAl_2O_4$ (ICSD #24491) (Fig. 8a). For the tested sample, the HRTEM images exhibit dispersed Cu nanoparticles which have an interplanar spacing of 2.09 Å corresponding to (111) plane of cubic Cu (ICSD #53247) (Fig. 8b). This result further demonstrates the formation of Cu NPs during MSR. However, it is difficult to measure Cu particle size distribution from HRTEM images of the tested sample (Fig. 8b), because Cu NPs would shift and eventually disappear by prolonging the irradiation of electron beam or would be destroyed by a strong electron beam (Fig. S4). Therefore, a pre-oxidation treatment is performed on the tested sample aiming to transform Cu into divalent CuO, then the CuO particle sizes can be obtained and used to calculate the Cu particle size distribution.

As shown in Fig. 8c, the lattice fringes with an interplanar spacing of 2.52 Å are assigned to the ($\bar{1}$11) plane of CuO (ICSD #87124) which owns a monoclinic structure, as also supported by the XRD pattern of the pre-oxidized sample tested for 100 h (Fig. S5). Based on the enlarged image (Fig. 8d), the size of CuO particles can be measured, and then calibrated to Cu NPs sizes in the light of crystal structure and cell parameter of CuO (ICSD #87124) and Cu (ICSD #53247) (see supplementary material for the method, Fig. S6). As can be seen in Fig. 8d, the Cu NPs in the tested sample of 100 h show a size range of 4.0–12.0 nm, and the average copper size is determined to be 9.1 nm, which is lower

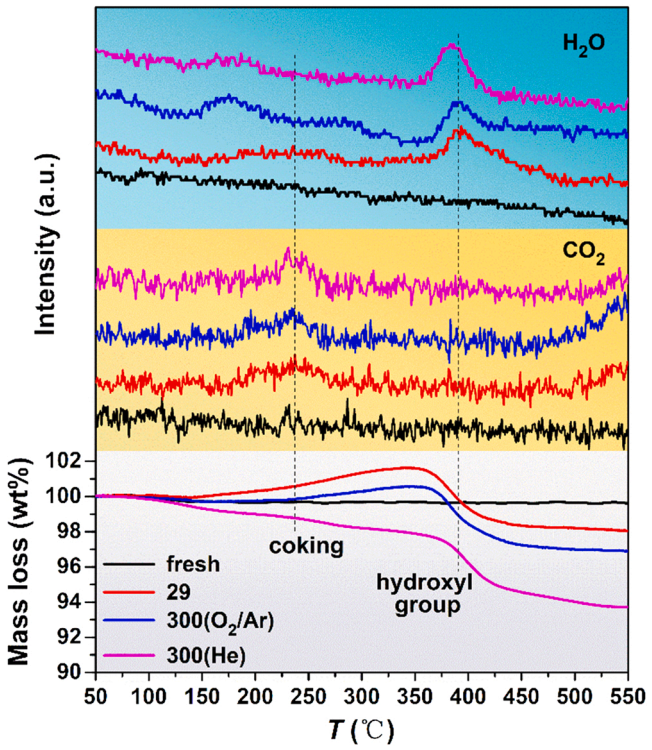

Fig. 9. TG-MS profiles of the fresh sample and tested samples with different *TOS*.

than the data obtained from XRD method (10.4 nm), but a little bigger than that measured by N_2O titration method (8.5 nm). The difference may be attributed to the distinct mechanism of XRD, N_2O titration and HRTEM methods in characterizing Cu entities. Importantly, we believe that the copper size obtained by N_2O titration method is closer to the real state because N_2O is capable to capture separated Cu atoms or small Cu clusters, as also indicated by previous researchers [61]. In summary, Cu NPs with wide size distribution are generated in situ via the sustained release of Cu from the $CuAl_2O_4$ spinel in MSR.

3.5. Coking and physisorption analysis

3.5.1. TG-MS studies

TG-MS technique is used to characterize the possible coke formation in tested spinel samples using 5% O_2/Ar as the carrier gas. For comparison reasons, Helium is also used for the 300 h tested sample. Prior to TG-MS analysis, all samples are treated in 5% O_2/Ar (at 50 °C for 1 h) to remove most of the adsorbed water.

As shown in Fig. 9, the samples heated up in 5% O_2/Ar show distinct differences in their weight change behavior. With the fresh spinel sample, only a slight mass loss occurs in the low temperature range of 80–140 °C, owing to the desorption of strong physical adsorbed water. However, the two tested samples demonstrate big mass changes both in O_2/Ar and He. It is found that the 29 h and 300 h samples show obvious mass increases between 130 and 350 °C and followed by mass losses when heated in O_2/Ar. This is because divalent spinel Cu^{2+} will transform into Cu metal after MSR reaction, and the oxidation of copper metal to CuO leads to the mass increases. Further evidence supports this point since the 300 h sample treated in helium shows no mass increase.

The TG effluent goes into a mass spectrometer to detect key components such as CO_2 and H_2O. The CO_2 signal shows a peak in the temperature range of 180–270 °C for all tested samples, owing to the decomposition of carbon deposit. According to literature results [62–64], the carbon deposit on Cu catalysts in MSR is mainly formate species (HCOO-) adsorbed on the catalyst surface. The amount of carbon deposit, quantified by the inner standardization method with graphite, increases gradually with prolonged reaction time (Table S5). The coking rate shows an increase before 7 h and a decrease after that, and becomes extremely lower after 29 h (Fig. S7). The measured average coking rate between 29 and 300 h is 2.21×10^{-4} wt% h^{-1}.

Importantly, a sharp H_2O signal appeared at about 375 °C with all tested samples except the fresh sample, and this accounts well for the obvious mass loss. which is observed in the corresponding temperature range. Since no CO_2 apparent peak is found, this H_2O peak can be attributed to the dehydration of hydroxyl group formed in defect spinel during MSR [59].

3.5.2. N_2 Physisorption analysis

N_2 Physisorption Analysis is performed to measure surface areas, pore volumes, and pore diameters of catalysts. The surface area of spinel samples varies between 12.3 and 21.7 m^2 g^{-1} up to 300 h *TOS* (Table S5). Specifically, in the first 5 h the surface area decreases from 19.9 m^2 g^{-1} to 12.3 m^2 g^{-1}, while from 5 h to 300 h it increases up to 21.7 m^2 g^{-1}. Pore analysis shows that all samples are featured by a broad pore size distribution of 2.0–60 nm, which is typical for mesoporous materials (Fig. S8). The pore volume shows an increase from 0.103 cm^3 g^{-1} to 0.156 cm^3 g^{-1} in the first 29 h, which is followed by a gradual decrease to 0.115 cm^3 g^{-1} in the *TOS* range of 29–300 h (Table S5). The variation of BET surface area and pore volume may have connections with copper releasing, catalyst structure evolution and coking, showing a complicated effect.

4. Discussion

4.1. Releasing features of spinel Cu

As shown in our previous studies, the as-synthesized Cu-Al spinel oxides can be used directly as an efficient catalyst in MSR reaction [37]. It has been well documented that the non-spinel CuO can be reduced to Cu metal by methanol at a low temperature of 225 °C, playing a crucial role in initiating the MSR reaction. Then gradual release of Cu from spinel lattice takes place, forming more active Cu sites to drive the reaction [37,39]. Once the reaction is initiated at atmospheric pressure, product gases (including H_2 and CO_2 mainly) will accumulate gradually in the reaction system, leading to an increase in reaction pressure up to 1.0 MPa. The time needed in this stage is about 4 h with the $CuAl_2O_4$ spinel catalyst.

As can be seen in Table 1 and Fig. S9, the Cu releasing rate is relatively low during the initial 0–4 h period, and reaches a maximum at 5 h and then declines gradually thereafter. The initial low releasing rate is due to the low hydrogen concentration. With the *TOS* increasing, the formation of hydrogen is accelerated by more liberated active Cu, thus leading to an increased average releasing rate of spinel Cu^{2+} during 4–5 h. Afterwards, the releasing rate drops consistently and it drops sharply after 29 h when most spinel Cu^{2+} ions (91.1%) have been liberated. Specifically, the average releasing rate is 0.025% h^{-1} between 29 and 100 h and becomes 0.0065% h^{-1} within 100–300 h, respectively.

It should be noted that only 94.2% of the spinel Cu^{2+} ions can be released up to 300 h, and about 5.8% Cu^{2+} ions remain in spinel lattice, which is verified by the presence of the spinel reduction peak in the H_2-TPR profile (Fig. 3). However, XPS results show that the surface spinel Cu^{2+} is about 9.9%, which is larger than the bulk value of 5.8%. These results indicates that most remnant spinel Cu^{2+} situate in catalyst surface layers, forming Cu-deficient defect spinel on which the released Cu entities are anchored.

The released Cu atoms will agglomerate to Cu NPs during the MSR reaction, which is co-evidenced by XRD, N_2O titration and HRTEM methods. The average crystallite size of Cu NPs shows a decrease before 29 h (XRD and N_2O titration results), which can be accounted for by the formation of more Cu NPs with even smaller sizes. To further investigate

Table 3
Comparison of Cu NPs diameter obtained via SRC and conventional pre-reduction method.

Catalysts	Catalyst using methods	Reduction conditions	d_{Cu}^{XRD} (nm)	Ref.
$CuAl_2O_4$	SRC	/	10.3–11.0	This work
Cu-Al spinel	SRC	/	8.5–18.3	[37]
Cu-Ni-Al spinel	SRC	/	7.7–10.3	[38]
Cu-Mg-Al spinel	SRC	/	8.1–9.5	[43]
$CuFe_2O_4$ and γ-Al_2O_3	Pre-reduction	H_2, 250–650 °C	24.0–60.0	[30]
$CuFe_2O_4$	Pre-reduction	H_2, 300 °C	3.6–30.6	[65]
CuMn-spinel	Pre-reduction	H_2, 250 °C	11.0	[66]
CuZnZr(Ce)/Al_2O_3	Pre-reduction	H_2, 300 °C	15.5–36.4	[67]
Cu/SiO_2 and ZnO-Cu/SiO_2	Pre-reduction	H_2, 250 °C	29.0–39.0	[68]

this phenomenon, the number of Cu NPs is calculated (see supplementary material for the calculation method) and plotted versus *RD*. A quasi-linear increasing relationship is observed between the Cu NPs number and *RD* (Fig. S10), and the slope means the amount of newly formed Cu NPs with the incremental releasing of spinel copper.

To give an insight into the differences between SRC and conventional pre-reduction method, XRD experiments were carried out on the $CuAl_2O_4$ spinel sample pre-reduced from *RT* to 260 °C, 430 °C, 550 °C, 650 °C and 800 °C. The calculated average Cu NPs size increases from 10.2 nm to 13.8 nm (Fig. S11), showing a severer agglomerating effect as compared to SRC method. This result indicates that the in-situ generation of active Cu via SRC method during MSR reaction is superior to hydrogen pre-reduction method for obtaining smaller Cu NPs, and hence ultimately affects the catalytic performance as indicated in our previous paper [37]. Moreover, some literature results using pre-reduction methods and our recent results using SRC method are summarized in Table 3. It is clear that the Cu NPs obtained via SRC method are generally smaller than that from pre-reduction method.

4.2. Structural revolution of Cu-Al spinel

It is illustrated that the frame of Cu-Al spinel remains unchanged as the face-centered cubic structure during the sustained release catalysis in MSR. Moreover, XRD experiments on pre-reduced $CuAl_2O_4$ spinel indicate that Cu-Al spinel frame keeps stable even at a high reduction temperature of 800 °C (Fig. S11), demonstrating the superior stability of Cu-Al spinel frame.

Interestingly, spinel Cu^{2+} and Al^{3+} cations redistribute between tetrahedral and octahedral interstices when Cu atoms are released from spinel structure. With the fresh stoichiometric spinel $CuAl_2O_4$, the spinel Cu^{2+} distribution (Cu_{Td}/Cu_{Oh}) in catalyst out-layer is measured to be 75.5/24.3 (Table S2), which is close to the bulk results of 80/20 determined by EXAFS and XRD refinement method in our previous work [44]. As can be expected, the release of spinel Cu^{2+} ions leads to the formation of cation deficiency spinel with respect to Cu^{2+}. Hence, a series of defective Cu-Al spinels are formed during the releasing process in MSR, which can be depicted as the following:

$$CuAl_2O_4 \rightarrow 3xCu + Cu_{1-3x}V_xAl_{2+2x}O_4 \ (V\text{: Vacancy})$$

The value of x becomes bigger with increasing *TOS* (Table 2). It's worth noting that at 300 h about 10% spinel Cu^{2+} ions remain in the out-layer while only 5.8% in bulk, illustrating that most of remnant spinel Cu^{2+} reside in the out-layer of tested defect spinel. Based on our previous experimental [39] and theoretical [53] studies, it is speculated that the formed surface defect spinel can stabilize the released copper entities as evidenced by stable sizes of Cu NPs and superior catalytic performance as compared with CuO/γ-Al_2O_3 in MSR. Thus, we believe that new vacancy sites, generated on defect spinel surfaces during the sustained releasing process, might play a crucial role in anchoring the newly formed Cu NPs.

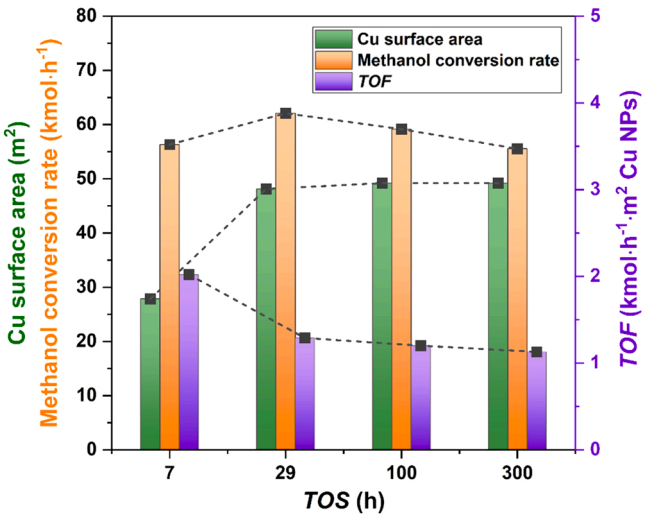

Fig. 10. Total Cu surface area, methanol conversion rate and turnover frequency versus *TOS*.

For Cu-Al spinel, it is assumed that the bulk cation distribution is close to the catalyst surface, illustrated by K.-i. Shimizu previously [47]. The structural formula of Cu-Al spinel can be written as $(Cu_{1-y}Al_y)[Cu_yAl_{2-y}]O_4$ in which parentheses and brackets stands for tetrahedral and octahedral interstices, respectively. According to the principle that octahedral cations have a double number of tetrahedral cations, the distribution of spinel vacancies can be calculated based on the Cu^{2+} and Al^{3+} ions distribution. The results show that the vacancies mainly exist in tetrahedral interstices of the spinel structure during the releasing process, and the spinel structural formulas at different *TOS* are given in Table S6.

4.3. Clarification for catalytic behavior of the $CuAl_2O_4$ sample

Without a pre-reduction treatment, the catalytic activity of the stoichiometric $CuAl_2O_4$ spinel in MSR shows a slight increase during the very beginning 29 h, then slowly decreases from 29 h to 300 h [39]. The initial activity rise should attribute to the quick releasing of spinel Cu^{2+} ions, which provides new active Cu NPs. From 29–300 h, coke deposition may primarily account for the activity declines.

As can be seen in Fig. 10, the total Cu surface area, calculated from specific Cu surface area (N_2O titration result) and releasing degree of Cu (H_2-TPR result), shows a sharp increase from 7 h to 29 h due to the quick release of spinel Cu, and a slight increase during 29–300 h owing to the lower releasing rate of spinel Cu (Table 1). The turnover frequency (*TOF*), denoted as the methanol conversion rates per square meter Cu NPs, is calculated. Interestingly, it is found that the *TOF* shows a decreasing trend with *TOS*, characterized by a quick decline from 7 h to 29 h and a slight decrease from 29–300 h. The observed feature is coincident with the variation of coking rate (Fig. S7). Hence, it is postulated that partial Cu NPs might be blocked by coke deposition, resulting in the decreased *TOF* value. From 29–300 h, the Cu surface area increases slightly, but the conversion rate shows an opposite trend, probably suggesting the local structure of Cu surface varies during the sustained release process which requires further investigations.

4.4. Dynamics of sustained release process

As a dynamic process in catalysis, the sustained release of Cu from Cu-Al spinel in MSR shows some dynamic features as summarized below. As illustrated in our previous work [37], the non-spinel CuO

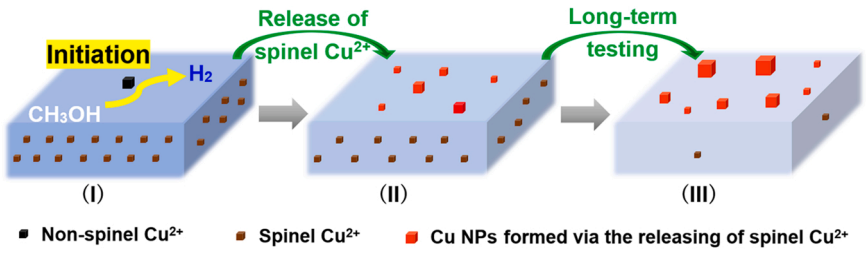

Fig. 11. The proposed schematic diagram of sustained release catalysis with the $CuAl_2O_4$ spinel catalyst.

species in the catalyst are easily reduced by methanol and play a crucial role in initiating the MSR reaction. When the reaction is initiated, spinel Cu will be gradually released from spine structure with *TOS*, resulting in the formation of Cu nano-particles and Cu-deficient Cu-Al spinel. The formed Cu NPs via in-situ releasing of spinel Cu are stabilized on the surface of the defect spinel, giving rise to superior catalytic stability. Based on the above information, a schematic diagram of SRC for the stoichiometric $CuAl_2O_4$ spinel has been proposed. As shown in Fig. 11, three typical stages have been suggested. The stage I stands for the initiation process of the MSR that non-spinel CuO will react initially with methanol to form H_2, then hydrogen can accelerate the releasing of spinel Cu^{2+} ions (stage II) to active Cu, which in turn contribute to the generation of hydrogen from methanol. After a long-term testing, a majority of spinel Cu^{2+} ions will be released and transformed into Cu NPs with a wide size distribution (stage III). Importantly, a small amount of Cu^{2+} ions still remain in spinel lattice and mainly locate in surface defect spinel which is believed to play a crucial role in anchoring the active Cu entities.

In a word, using SRC method, active Cu atoms are in situ released gradually from spinel structure, and the remnant surface spinel can well support the Cu entities, giving a dramatical increase of catalytic activity and stability in MSR than conventional pre-reduction methods. This result can provide guide in designing catalyst utilization strategy in other catalytic systems.

5. Conclusions

The dynamic releasing of Cu^{2+} from a stoichiometric $CuAl_2O_4$ spinel in methanol steam reforming without catalyst pre-reduction treatment has been examined by comprehensive characterizations of six tested samples with different *TOS*. The releasing rate of Cu^{2+} from spinel lattice increases first and then decreases sharply with *TOS*. The released copper atoms agglomerate to nano-particles and/or clusters, showing a relatively stable crystallite size within 8.5–9.3 nm. Simultaneously, a series of Cu-deficient defect spinels are formed during the releasing process, in which the cation redistribution in tetrahedral and octahedral interstices occurs. A small percentage of Cu^{2+} (5.8%) still remain in the crystal lattice even at a long *TOS* of 300 h, and they exist mainly in the surface layer. The formed defect spinels are believed to play a key role in stabilizing the in-situ formed Cu entities during the MSR reaction. These findings show the dynamic nature of the $CuAl_2O_4$ spinel catalyst in terms of both the active Cu and support structure, demonstrating that the sustained release catalysis is essentially different from the conventional metal catalytic systems.

CRediT authorship contribution statement

Ya-Jie Liu: Conceptualization, Investigation, Data curation, Writing – original draft, Funding acquisition. **He-Fei Kang:** Methodology, Investigation, Data curation, Writing – original draft. **Xiao-Ning Hou:** Software. **Shao-Jun Qing:** Resources. **Lei Zhang:** Visualization. **Zhi-Xian Gao:** Conceptualization, Supervision, Writing – review & editing, Funding acquisition. **Hong-Wei Xiang:** Resources.

Declaration of Competing Interest

The authors declare the following financial interests/personal relationships which may be considered as potential competing interests: Yajie Liu reports financial support was provided by National Natural Science Foundation of China and Natural Science Foundation for Young Scientists of Shanxi Province of China. Zhixian Gao reports financial support was provided by National Natural Science Foundation of China.

Data Availability

Data will be made available on request.

Acknowledgments

This work is supported by the Natural Science Foundation for Young Scientists of Shanxi Province of China (Grant No.: 20210302123358), and the National Natural Science Foundation of China (Grant No.: 21673270, 22202093).

Associated content

The supplementary material includes the full width at half maxima of reduction peaks; XRD characterization data of Cu-Al spinel cell constant; simulation data of Cu L_3-edge XANES spectra; simulation data of ^{27}Al MAS NMR spectra; characterization results of Cu properties by N_2O titration method; supplementary HRTEM images on tested Cu-Al spinel with a *TOS* of 100 h; calculation methods of Cu size from CuO crystal information; coking and physisorption analysis data; average releasing rate versus releasing degree (*RD*) and *TOS*; calculation methods of Cu NPs number in terms of releasing degree of spinel Cu; XRD data of reduced Cu-Al spinel catalysts.

Appendix A. Supporting information

Supplementary data associated with this article can be found in the online version at doi:10.1016/j.apcatb.2022.122043.

References

[1] M.B. Gawande, A. Goswami, F.X. Felpin, T. Asefa, X. Huang, R. Silva, X. Zou, R. Zboril, R.S. Varma, Cu and Cu-based nanoparticles: synthesis and applications in catalysis, Chem. Rev. 116 (2016) 3722–3811, https://doi.org/10.1021/acs.chemrev.5b00482.

[2] A.-a Ye, Z.-r Li, J.-q Ding, W. Xiong, W.-x Huang, Synergistic catalysis of Al and Zn sites of spinel $ZnAl_2O_4$ catalyst for CO hydrogenation to methanol and dimethyl ether, ACS Catal. 11 (2021) 10014–10019, https://doi.org/10.1021/acscatal.1c02742.

[3] H.-q Song, D. Laudenschleger, J.J. Carey, H. Ruland, M. Nolan, M. Muhler, Spinel-structured $ZnCr_2O_4$ with excess Zn is the active ZnO/Cr_2O_3 catalyst for high-temperature methanol synthesis, ACS Catal. 7 (2017) 7610–7622, https://doi.org/10.1021/acscatal.7b01822.

[4] T.-k Liu, D. Xu, D.-d Wu, G.-l Liu, X.-l Hong, Spinel $ZnFe_2O_4$ regulates copper sites for CO_2 hydrogenation to methanol, ACS Sustain. Chem. Eng. 9 (2021) 4033–4041, https://doi.org/10.1021/acssuschemeng.0c07682.

[5] S.T. Yong, C.W. Ooi, S.P. Chai, X.S. Wu, Review of methanol reforming-Cu-based catalysts, surface reaction mechanisms, and reaction schemes, Int. J. Hydrog. Energ. 38 (2013) 9541–9552, https://doi.org/10.1016/j.ijhydene.2013.03.023.

[6] S. Zhang, S.-j Liu, X.-c Zhu, Y. Yang, W.-s Hu, H.-t Zhao, R.-y Qu, C.-h Zheng, X. Gao, Low temperature catalytic oxidation of propane over cobalt-cerium spinel oxides catalysts, Appl. Surf. Sci. 479 (2019) 1132–1140, https://doi.org/10.1016/j.apsusc.2019.02.118.

[7] J.-c Wu, Y.-z Li, Y. Yang, Q. Zhang, L. Yun, S.-w Wu, C.-y Zhou, Z.-k Jiang, X.-j Zhao, A heterogeneous single Cu catalyst of Cu atoms confined in the spinel lattice of $MgAl_2O_4$ with good catalytic activity and stability for NO reduction by CO, J. Mater. Chem. A 7 (2019) 7202–7212, https://doi.org/10.1039/C8TA11528A.

[8] A.M. Bahmanpour, F. Héroguel, M. Kılıç, C.J. Baranowski, L. Artiglia, U. Röthlisberger, J.S. Luterbacher, O. Kröcher, Cu-Al spinel as a highly active and stable catalyst for the reverse water gas shift reaction, ACS Catal. 9 (2019) 6243–6251, https://doi.org/10.1021/acscatal.9b01822.

[9] K. Faungnawakij, R. Kikuchi, N. Shimoda, T. Fukunaga, K. Eguchi, Effect of thermal treatment on activity and durability of $CuFe_2O_4$-Al_2O_3 composite catalysts for steam reforming of dimethyl ether, Angew. Chem. Int. Ed. 47 (2008) 9314–9317, https://doi.org/10.1002/anie.200802809.

[10] G.O. Larrazábal, A.J. Martín, S. Mitchell, R. Hauert, J. Pérez-Ramírez, Enhanced reduction of CO_2 to CO over Cu-In electrocatalysts: catalyst evolution is the key, ACS Catal. 6 (2016) 6265–6274, https://doi.org/10.1021/acscatal.6b02067.

[11] H.N. Abdelhamid, Delafossite nanoparticle as new functional materials: advances in energy, nanomedicine and environmental applications, Mater. Sci. Forum 832 (2015) 28–53, https://doi.org/10.4028/www.scientific.net/MSF.832.28.

[12] A.P. Amrute, G.O. Larrazabal, C. Mondelli, J. Perez-Ramirez, $CuCrO_2$ delafossite: a stable copper catalyst for chlorine production, Angew. Chem. Int. Ed. 52 (2013) 9772–9775, https://doi.org/10.1002/anie.201304254.

[13] Y.-n Yi, H. Liu, B.-x Chu, Z.-z Qin, L.-h Dong, H.-x He, C.-j Tang, M.-g Fan, L. Bin, Catalytic removal NO by CO over $LaNi_{0.5}M_{0.5}O_3$ (M = Co, Mn, Cu) perovskite oxide catalysts: Tune surface chemical composition to improve N_2 selectivity, Chem. Eng. J. 369 (2019) 511–521, https://doi.org/10.1016/j.cej.2019.03.066.

[14] Q.-l Yang, G.-l Liu, Y. Liu, Perovskite-type oxides as the catalyst precursors for preparing supported metallic nanocatalysts: a review, Ind. Eng. Chem. Res. 57 (2018) 1–17, https://doi.org/10.1021/acs.iecr.7b03251.

[15] M. Ao, G.H. Pham, V. Sage, V. Pareek, S.-M. Liu, Perovskite-derived trimetallic Co-Ni-Cu catalyst for higher alcohol synthesis from syngas, Fuel Process Technol. 193 (2019) 141–148, https://doi.org/10.1016/j.fuproc.2019.05.002.

[16] W. Kim, K.K. Mohaideen, D.J. Seo, W.L. Yoon, Methanol-steam reforming reaction over Cu-Al-based catalysts derived from layered double hydroxides, Int. J. Hydrog. Energ. 42 (2017) 2081–2087, https://doi.org/10.1016/j.ijhydene.2016.11.014.

[17] G.-l Fan, F. Li, D.G. Evans, X. Duan, Catalytic applications of layered double hydroxides: recent advances and perspectives, Chem. Soc. Rev. 43 (2014) 7040–7066, https://doi.org/10.1039/c4cs00160e.

[18] S.R. Segal, K.B. Anderson, K.A. Carrado, C.L. Marshall, Low temperature steam reforming of methanol over layered double hydroxide-derived catalysts, Appl. Catal. A Gen. 231 (2002) 215–226, https://doi.org/10.1016/S0926-860X(02)00055-8.

[19] A. Alejandre, F. Medina, X. Rodriguez, P. Salagre, Y. Cesteros, J.E. Sueiras, Cu/Ni/Al layered double hydroxides as precursors of catalysts for the wet air oxidation of phenol aqueous solutions, Appl. Catal. B Environ. 30 (2001) 195–207, https://doi.org/10.1016/S0926-3373(00)00233-2.

[20] S. Velu, K. Suzuki, T. Osaki, Selective production of hydrogen by partial oxidation of methanol over catalysts derived from CuZnAl-layered double hydroxides, Catal. Lett. 62 (1999) 159–167, https://doi.org/10.1023/A:1019023811688.

[21] M. Behrens, F. Studt, I. Kasatkin, S. Kühl, M. Hävecker, F. Abild-Pedersen, S. Zander, F. Girgsdies, P. Kurr, B.L. Kniep, M. Tovar, R.W. Fischer, J.K. Nørskov, R. Schlögl, The active site of methanol synthesis over $Cu/ZnO/Al_2O_3$ industrial catalysts, Science 336 (2012) 893–897, https://doi.org/10.1126/science.1219831.

[22] J.-l Gong, H.-r Yue, Y.-j Zhao, S. Zhao, L. Zhao, J. Lv, S.-p Wang, X.-b Ma, Synthesis of ethanol via syngas on Cu/SiO_2 catalysts with balanced Cu^0-Cu^+ sites, J. Am. Chem. Soc. 134 (2012) 13922–13925, https://doi.org/10.1021/ja3034153.

[23] S. Natesakhawat, J.W. Lekse, J.P. Baltrus, P.R. Ohodnicki, B.H. Howard, X. Deng, C. Matranga, Active sites and structure-activity relationships of copper-based catalysts for carbon dioxide hydrogenation to methanol, ACS Catal. 2 (2012) 1667–1676, https://doi.org/10.1021/cs300008g.

[24] S. Kattel, P.J. Ramírez, J.G. Chen, J.A. Rodriguez, P. Liu, Active sites for CO_2 hydrogenation to methanol on Cu/ZnO catalysts, Science 355 (2017) 1296–1299, https://doi.org/10.1126/science.aal3573.

[25] F. Bossola, N. Scotti, F. Somodi, M. Coduri, C. Evangelisti, V. Dal Santo, Electron-poor copper nanoparticles over amorphous zirconia-silica as all-in-one catalytic sites for the methanol steam reforming, Appl. Catal. B: Environ. 258 (2019), 118016, https://doi.org/10.1016/j.apcatb.2019.118016.

[26] W.-W. Wang, P.-P. Du, S.-H. Zou, H.-Y. He, R.-X. Wang, Z. Jin, S. Shi, Y.-Y. Huang, R. Si, Q.-S. Song, C.-J. Jia, C.-H. Yan, Highly dispersed copper oxide clusters as active species in copper-ceria catalyst for preferential oxidation of carbon monoxide, ACS Catal. 5 (2015) 2088–2099, https://doi.org/10.1021/cs5014909.

[27] H.-h Yang, Y.-y Chen, X.-j Cui, G.-f Wang, Y.-l Cen, T.-s Deng, W.-j Yan, J. Gao, S.-h Zhu, U. Olsbye, J.-g Wang, W.-b Fan, A highly stable Cu-based catalyst for clarifying the catalytic roles of Cu^0 and Cu^+ species in methanol dehydrogenation, Angew. Chem. Int. Ed. 130 (2018) 1854–1858, https://doi.org/10.1002/ange.201710605.

[28] Y. Tanaka, T. Utaka, R. Kikuchi, K. Sasaki, K. Eguchi, Water gas shift reaction over Cu-based mixed oxides for CO removal from the reformed fuels, Appl. Catal. A: Gen. 242 (2003) 287–295, https://doi.org/10.1016/S0926-860X(02)00529-X.

[29] L.-y Guo, J.-x Zhou, J.-b Mao, X.-w Guo, S.-g Zhang, Supported Cu catalysts for the selective hydrogenolysis of glycerol to propanediols, Appl. Catal. A: Gen. 367 (2009) 93–98, https://doi.org/10.1016/j.apcata.2009.07.040.

[30] K. Faungnawakij, R. Kikuchi, T. Fukunaga, K. Eguchi, Catalytic hydrogen production from dimethyl ether over $CuFe_2O_4$ spinel-based composites: Hydrogen reduction and metal dopant effects, Catal. Today 138 (2008) 157–161, https://doi.org/10.1016/j.cattod.2008.05.004.

[31] F. Severino, J.L. Brito, J. Laine, A. López-Agudo, J.L.G. Fierro, Nature of copper active sites in the carbon monoxide oxidation on $CuAl_2O_4$ and $CuCr_2O_4$ spinel type catalysts, J. Catal. 177 (1998) 82–95, https://doi.org/10.1006/jcat.1998.2094.

[32] J. Laine, F. Severino, A. López-Agudo, J.L.G. Fierro, Structural changes in a Cu/Al_2O_3 catalyst when used for oxidation of carbon monoxide, J. Catal. 129 (1991) 297–299, https://doi.org/10.1016/0021-9517(91)90033-Z.

[33] J. Laine, F. Severino, A. Lopez-Agudo, J.L.G. Fierro, The effect of chromium on deactivation of alumina-supported copper catalysts, Stud. Surf. Sci. Catal. 68 (1991) 467–473, https://doi.org/10.1016/S0167-2991(08)62670-1.

[34] D.S. Brands, E.K. Poels, T.A. Krieger, O.V. Makarova, C. Weber, S. Veer, A. Bliek, The relation between reduction temperature and activity in copper catalysed ester hydrogenolysis and methanol synthesis, Catal. Lett. 36 (1996) 175–182, https://doi.org/10.1007/BF00807616.

[35] T. Shishido, M. Yamamoto, D. Li, Y. Tian, H. Morioka, M. Honda, T. Sano, K. Takehira, Water-gas shift reaction over Cu/ZnO and $Cu/ZnO/Al_2O_3$ catalysts prepared by homogeneous precipitation, Appl. Catal. A Gen. 303 (2006) 62–71, https://doi.org/10.1016/j.apcata.2006.01.031.

[36] C.J.G. Van Der Grift, A.F.H. Wielers, B.P.J. Jogh, J.V. Beunum, M.D. Boer, M. Versluijs-Helder, J.W. Geus, Effect of the reduction treatment on the structure and reactivity of silica-supported copper particles, J. Catal. 131 (1991) 178–189, https://doi.org/10.1016/0021-9517(91)90334-Z.

[37] H.-j Xi, X.-n Hou, Y.-j Liu, S.-j Qing, Z.-x Gao, Cu-Al spinel oxide as an efficient catalyst for methanol steam reforming, Angew. Chem. Int. Ed. 53 (2014) 11886–11889, https://doi.org/10.1002/anie.201405213.

[38] Y.-j Liu, S.-j Qing, X.-n Hou, F.-j Qin, X. Wang, Z.-x Gao, H.-w Xiang, Cu-Ni-Al spinel oxide as an efficient durable catalyst for methanol steam reforming, ChemCatChem 10 (2018) 5698–5706, https://doi.org/10.1002/cctc.201801472.

[39] Y.-j Liu, S.-j Qing, X.-n Hou, F.-j Qin, X. Wang, Z.-x Gao, H.-w Xiang, Temperature dependence of Cu-Al spinel formation and its catalytic performance in methanol steam reforming, Catal. Sci. Technol. 7 (2017) 5069–5078, https://doi.org/10.1039/c7cy01236e.

[40] S.-j Qing, X.-n Hou, Y.-j Liu, L.-d Li, X. Wang, Z.-x Gao, W.-b Fan, Strategic use of $CuAlO_2$ as a sustained release catalyst for production of hydrogen from methanol steam reforming, Chem. Commun. 54 (2018) 12242–12245, https://doi.org/10.1039/c8cc06600k.

[41] Y.-j Liu, H.-f Kang, X.-n Hou, L. Zhang, S.-j Qing, Z.-x Gao, H.-w Xiang, Synthesis of Cu-Al spinels and its non-isothermal formation kinetics analysis, J. Fuel Chem. Technol. 48 (2020) 338–348, https://doi.org/10.3969/j.issn.0253-2409.2020.03.010.

[42] F.-j Qin, Y.-j Liu, S.-j Qing, X.-n Hou, Z.-x Gao, Cu-Al spinel as a sustained release catalyst for H_2 production from methanol steam reforming: Effects of different copper sources, J. Fuel. Chem. Technol. 45 (2017) 1481–1488, https://doi.org/10.1016/S1872-5813(17)30065-8.

[43] X.-n Hou, S.-j Qing, Y.-j Liu, L.-d Li, Z.-x Gao, Y. Qin, Enhancing effect of MgO modification of Cu-Al spinel oxide catalyst for methanol steam reforming, Int. J. Hydrog. Energ. 45 (2019) 477–489, https://doi.org/10.1016/j.ijhydene.2019.10.164.

[44] Y.-j Liu, S.-j Qing, X.-n Hou, G. Feng, R.-b Zhang, X. Wang, S.-m Wang, Z.-x Gao, H.-w Xiang, Synthesis and structural characterization of $CuAl_2O_4$ spinel with an unusual cation distribution, J. Mater. Appl. 7 (2018) 82–89, https://doi.org/10.32732/jma.

[45] K.E. Sickafus, J.M. Wills, Structure of spinel, J. Am. Ceram. Soc. 82 (1999) 3279–3292, https://doi.org/10.1111/j.1151-2916.1999.tb02241.x.

[46] M. Grioni, J.B. Goedkoop, R. Schoorl, F.M.F. de Groot, J.C. Fuggle, F. Schäfers, E. E. Koch, G. Rossi, J.M. Esteva, R.C. Karnatak, Studies of copper valence states with Cu L_3 x-ray-absorption spectroscopy, Phys. Rev. B 39 (1989) 1541–1545, https://doi.org/10.1103/PhysRevB.39.1541.

[47] K.-i Shimizu, H. Maeshima, H. Yoshida, A. Satsuma, T. Hattori, Spectroscopic characterisation of Cu-Al_2O_3 catalysts for selective catalytic reduction of NO with propene, Phys. Chem. Chem. Phys. 2 (2000) 2435–2439, https://doi.org/10.1039/B000943L.

[48] J.C. Klein, C.P. Li, D.M. Hercules, J.F. Black, Decomposition of copper compounds in x-ray photoelectron spectrometers, Appl. Spectrosc. 38 (1984) 729–734. ⟨https://opg.optica.org/as/abstract.cfm?uri=as-38-5-729#articleCitations⟩.

[49] R.T. Figueiredo, A. Martínez-Arias, M.L. Granados, J.L.G. Fierro, Spectroscopic evidence of Cu-Al interactions in Cu-Zn-Al mixed oxide catalysts used in CO hydrogenation, J. Catal. 178 (1998) 146–152, https://doi.org/10.1006/jcat.1998.2106.

[50] B.R. Strohmeier, D.E. Leyden, R.S. Field, D.M. Herculers, Surface spectroscopic characterization of Cu/Al_2O_3 catalysts, J. Catal. 94 (1985) 514–530, https://doi.org/10.1016/0021-9517(85)90216-7.

[51] G. Moretti, G. Fierro, M. Lo Jacono, P. Porta, Characterization of CuO-ZnO catalysts by x-ray photoelectron spectroscopy: precursors, calcined and reduced samples, Surf. Interface Anal. 14 (1989) 325–336, https://doi.org/10.1002/sia.740140609.

[52] S.F. Tikhov, V.A. Sadykov, G.N. Kryukova, E.A. Paukshtis, V.V. Popovskii, T. G. Starostina, G.V. Kharlamov, V.F. Anufrienko, V.F. Poluboyarov, V. A. Razdobarov, N.N. Bulgakov, A.V. Kalinkin, Microstructural and spectroscopic investigations of the supported copper-alumina oxide systtem: nature of aging in oxidizing reaction media, J. Catal. 134 (1992) 506–524, https://doi.org/10.1016/0021-9517(92)90338-I.

[53] L. Shi, D.-s Wang, X.-h Yu, L. Li, Z.-H. Lu, G. Feng, R.-b Zhang, S.-j Qing, Z.-x Gao, Q.-q Luo, Adsorption of Cu_n (n = 1-4) clusters on $CuAl_2O_4$ spinel surface: A DFT study, Mol. Catal. 468 (2019) 29–35, https://doi.org/10.1016/j.mcat.2019.02.009.

[54] T. James, M. Padmanabhan, K.G.K. Warrier, S. Sugunan, $CuAl_2O_4$ formation and its effect on α-Al_2O_3 phase evolution on calcination of metal ion doped boehmite xerogels, Mater. Chem. Phys. 103 (2007) 248–254, https://doi.org/10.1016/j.matchemphys.2007.02.022.

[55] K. Okada, A. Hattori, T. Taniguchi, A. Nukui, R.N. Das, Effect of effect of divalent cation additives on the γ-Al_2O_3-to-α-Al_2O_3 phase transition, J. Am. Ceram. Soc. 83 (2000) 928–932, https://doi.org/10.1111/j.1151-2916.2000.tb01296.x.

[56] H. Furuhashi, M. Inagaki, S. Naka, Determination of cation distribution in spinels by X-ray diffraction method, J. Inorg. Nucl. Chem. 35 (1973) 3009–3014, https://doi.org/10.1016/0022-1902(73)80531-7.

[57] K.-i Shimizu, H. Maeshima, H. Yoshida, A. Satsuma, T. Hattori, Crystal field effect on the chemical shift in Cu L_{III} XANES spectra of Cu(II) compounds, Chem. Lett. 29 (2000) 210–211, https://doi.org/10.1246/cl.2000.210.

[58] K.-i Shimizu, H. Maeshima, H. Yoshida, A. Satsuma, T. Hattori, Deconvolution analysis of Cu L-edge XANES for quantification of copper(II) coordinations in copper-aluminate catalysts (https://iopscience.iop.org/article/), Jpn. J. Appl. Phys. 38 (1999) 44–46, https://doi.org/10.7567/JJAPS.38S1.44/meta.

[59] L.M. Plyasova, T.M. Yur'eva, I.Y. Molina, T.A. Kriger, A.M. Balagurov, L. P. Davydova, V.I. Zaikovskii, G.N. Kustova, V.V. Malakhov, L.S. Dovlitova, Dynamics of structural transformations in the reduction of copper aluminate, Kinet. Catal. 41 (1998) 429–436, https://doi.org/10.1007/BF02755383.

[60] W.S. Xia, H.L. Wan, Y. Chen, Cluster model study on the surface interactions of γ-alumina-supported metal oxides, J. Mol. Catal. A Chem. 138 (1999) 185–195, https://doi.org/10.1016/S1381-1169(98)00145-9.

[61] Z.-l Yuan, L.-n Wang, J.-h Wang, S.-x Xia, P. Chen, Z.-y Hou, X.-m Zheng, Hydrogenolysis of glycerol over homogenously dispersed copper on solid base catalysts, Appl. Catal. B: Environ. 101 (2011) 431–440, https://doi.org/10.1016/j.apcatb.2010.10.013.

[62] D.H.S. Ying, R.J. Madix, Thermal desorption study of formic acid decomposition on a clean Cu(110) surface, J. Catal. 61 (1980) 48–56, https://doi.org/10.1016/0021-9517(80)90338-3.

[63] K.C. Waugh, Methanol synthesis, Catal. Today 15 (1992) 51–75, https://doi.org/10.1016/0920-5861(92)80122-4.

[64] B.A. Peppley, J.C. Amphlett, L.M. Kearns, R.F. Mann, Methanol-steam reforming on $Cu/ZnO/Al_2O_3$. Part 1: the reaction network, Appl. Catal. A Gen. 179 (1999) 21–29, https://doi.org/10.1016/S0926-860X(98)00298-1.

[65] S.-C. Yang, W.-N. Su, S.D. Lin, J. Rick, J.-H. Cheng, J.-Y. Liu, C.-J. Pan, D.-G. Liu, J.-F. Lee, T.-S. Chan, H.-S. Sheu, B.-J. Hwang, Preparation of nano-sized Cu from a rod-like $CuFe_2O_4$: Suitable for high performance catalytic applications, Appl. Catal. B Environ. 106 (2011) 650–656, https://doi.org/10.1016/j.apcatb.2011.06.030.

[66] T. Fukunaga, N. Ryumon, N. Ichikuni, S. Shimazu, Characterization of CuMn-spinel catalyst for methanol steam reforming, Catal. Commun. 10 (2009) 1800–1803, https://doi.org/10.1016/j.catcom.2009.06.001.

[67] S.D. Jones, H.E. Hagelin-Weaver, Steam reforming of methanol over CeO_2- and ZrO_2-promoted Cu-ZnO catalysts supported on nanoparticle Al_2O_3, Appl. Catal. B Environ. 90 (2009) 195–204, https://doi.org/10.1016/j.apcatb.2009.03.013.

[68] Y. Matsumura, H. Ishibe, Suppression of CO by-production in steam reforming of methanol by addition of zinc oxide to silica-supported copper catalyst, J. Catal. 268 (2009) 282–289, https://doi.org/10.1016/j.jcat.2009.09.026.